# PROCEEDINGS OF SPIE

# VERT-X: VERTical X-ray raster-scan facility for ATHENA calibration. The concept design.

Moretti, A., Pareschi, G., Uslenghi, M., Tordi, M., Bressan, R., et al.

**SPIE.**

# VERT-X: A VERTical X-ray raster-scan facility for ATHENA calibration. The concept design.

A. Moretti[a], G. Pareschi[a], M. Uslenghi[b], M.Tordi[c], R. Bressan[c], G. Valsecchi[d], F. Zocchi[d], P. Attina`[e], F. Amisano[e], G. Sironi[a], B. Salmaso[a], S. Basso[a], G. Tagliaferri[a], D. Spiga[a], N. La Palombara[b], M. Fiorini[b], F. Dury[c], M. Spinola[c], F. Marioni[d], G. Parissenti[e], G. Parodi[f], E. Wille[g], P. Corradi[g], M. Bavdaz[g], and I. Ferreira[g]

[a]INAF-Brera, via Brera 28, 20123 Milan, Italy
[b]INAF-IASF, via Corti 12, 20133 Milan, Italy
[c]EIE, Via Torino, 151 A 30172 Mestre (VE), Italy
[d]Media Lario, Via al Pascolo, 23842 Bosisio Parini (LC), Italy
[e]GP Advanced Projects, Via Tartaglia 14, 25064 Gussago (BS), Italy
[f]BCV, via Sant'Orsola 1, 20123 Milan, Italy
[g]ESA-ESTEC, Keplerlaan 1, 2201 AZ Noordwjik, The Netherlands

## ABSTRACT

Calibration of the ATHENA telescope is a critical aspect of the project and raises significant difficulties due to the unprecedented size, mass and focal length of the mirror assembly. The VERT-X project, financed by ESA and started in January 2019 by a Consortium led by INAF and which includes EIE, Media Lario Technologies, GPAP, and BCV Progetti, aims to design an innovative calibration facility. In the VERT-X design the parallel beam, needed for calibration, is produced placing a source in the focus of an X-ray collimator. This system is mounted on a raster-scan mechanism which covers the entire ATHENA optics. The compactness of the VERT-X design allows a vertical geometry for the ATHENA calibration facility, with several potential benefits with respect to the long horizontal tube calibration facilities.

**Keywords:** Astronomy, X-ray, optics, ATHENA, calibration, facility, design

## 1. INTRODUCTION

The Advanced Telescope for High Energy Astrophysics (ATHENA) is the second Large mission of the ESA Cosmic Vision Science program. The phase A study will be completed at the end of 2019, aiming at the adoption before the end of 2021, with the launch planned in 2031 (Ferreira et al. 2019, in this conference).

ATHENA will represent a powerful X-ray observatory for all astrophysics fields [1]. The ambition of the mission will be the study of the Universe hot baryonic components, from super massive black holes (SMBH) in the early Universe to galaxy clusters and their large structures. These goals will be achieved through the largest ever built X-ray mirror which will focus 0.2-12.0 keV photons on two state-of-the-art instruments for spatially resolved high resolution spectroscopy (the X-ray Integral Field Unit, X-IFU) and for wide field imaging and low resolution spectroscopy (the Wide Field Imager, WFI) respectively. The mirror will be built using the ESA Silicon Pore Optics (SPO) technology which provides large effective area with excellent angular resolution [2].

Testing and integration procedures of the single mirror modules (MM) have been already well established. X-rays measures will be done using monochromatic pencil-beams at the BESSY synchrotron and, then, in full illumination mode, using the BEATRIX testing facility [3]. The MM integration into the mirror assembly (MA) will be done using a large collimated UV beam, with a vertical facility that will be implemented ad hoc [4].

On the other hand, verification and calibration of the entire MA are particularly challenging and different options are under study. Indeed, the recommendation of the ATHENA telescope working group (TWG) is that

---

Send correspondence to A.M.
A.M.: E-mail: alberto.moretti@inaf.it
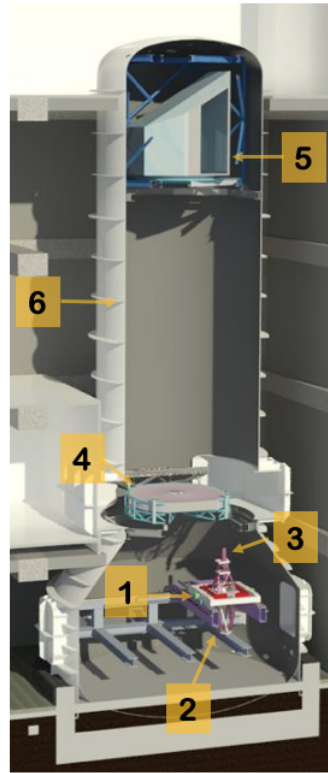
**1 Raster scan mechanism**

**2 X-ray source**

**3 Collimator**

**4 ATHENA mirror**

**5 Detector**

**6 Vacuum chamber**

Figure 1. The concept scheme of the VERT-X facility, with the subsystems labelled. In the focal plane the ATHENA science instrument module is designed. While this could be a possibility, the current baseline foresees a service detector, as explained in the text.

the source for verification and calibration of the MA should be located at a minimum distance of 300m with a goal of 800m [5]. Since the longest tube in Europe is the MPE Panter Lab [6], this can be realised only in a new X-ray long beam facility or by a significant upgrade of the NASA X-ray & Cryogenic Facility (XRCF, https://optics.msfc.nasa.gov/).

In this paper we describe the concept design of the VERTical X-ray raster-scan facility for ATHENA calibration (VERT-X) which has been thought to perform ground calibrations of the ATHENA MA producing an X-ray parallel beam without the need of positioning the X-ray source at such a long distance [7].

## 2. VERT-X CONCEPT

The VERT-X concept is based on the idea that a parallel beam can be also produced by a point-like source located in the focus of an error-free X-ray collimator. This concept is not novel and it is already under construction for the BEATRIX facility [3]. Since, for evident construction reasons, the beam amplitude has to be much smaller than the ATHENA mirror, the source-collimator system it is thought to be moved by a raster-scan mechanism which covers all the optics to be calibrated. This results in the design of a calibration facility much smaller in size (as shown in Fig.1) with respect to the traditional long tube.

Beside the smaller amount of involved resources, there are also other evident benefits generated by the compactness of this concept. First, it allows a vertical geometry which largely simplifies the mirror support and reduces to zero the PSF degradation due to the lateral (perpendicular to optical axis) gravity. This would also allow to host the MA integrated with the SIM in order to perform the end-to-end calibration campaign, although, at the moment this is not foreseen in the ATHENA project development schedule. Then, thanks to the compact

design, the location of the facility can be chosen flexibly and according to the project needs. Moreover, while the raster-scan mechanism introduces a time scale for the calibration operations (we will see that this is relatively short, i.e. $\sim 2.5$ hours), it allows to characterise the contribution of the single modules to the over-all mirror performance.

## 3. VERT-X DESIGN COMPONENTS

In the following sections we present the subsystems of the facility design: source, collimator, raster-scan, mirror support system and detector (Fig.1).

### 3.1 Raster-scan

The raster-scan mechanism aims at moving the collimated X-ray beam on the horizontal plane and tilting it around the two horizontal axes. Fig.2 shows a 3D view with the main components highlighted: they are the base, the bridge, the trolley, Gimbal and Serrurier supports, which are all designed in stainless steel.

Raster-scan can be divided into two logical parts. (i) the lower part from the base to the Gimbal mount, which is thought to bear, position and orient the X-ray beam with the required accuracy. The main elements of this part are the four motion axes that translate and rotate the beam (see below). (ii) The upper part with the Serrurier, which carries the X-ray source and the collimator. This part is thought to be as rigid and light as possible: rigidity maintains the alignment between X-ray source and collimator, while lightness simplifies the work of the underlying motion axes.
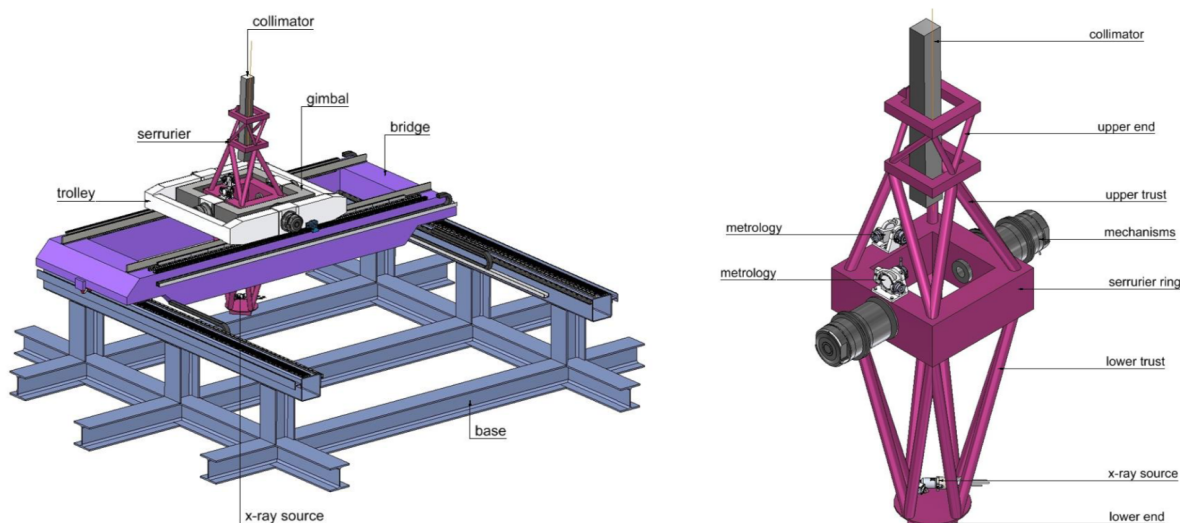


Figure 2. **Left panel:** 3D view of the raster-scan mechanism with the main parts highlighted. **Right panel:** Close up of the Serrurier.

The **base** is the fixed part of the raster-scan, the one supporting the translating bridge. It lays on rigid points of the vessel, in such a way to discharge the loads directly on the vessel foundations. The base hosts the rails onto which the Bridge slides, the magnets of the linear motors that push the bridge, and the tape of the bridge encoder.

The **bridge** is the first moving part of the raster-scan (translation along X). It slides over the base and it hosts the rails, the motor magnets, and the encoder tape for the trolley. The **trolley** is the second moving part of the raster-scan (translation along Y). It slides over the bridge and it constitutes the fixed part of the Gimbal mount. The **Gimbal** mount allows the Serrurier truss (which carries the X-ray beam) to rotate around X and Y axes. Technically, the Gimbal is a Cardan suspension with the two rotation axes converging on the same point, which prevents the Serrurier axis to offset while rotating. In order to have the Gimbal perfectly balanced, the centre of rotation shall also be the centre of gravity of the Serrurier truss. Possible unbalances will be corrected by

dedicated counterweights. The **Serrurier**, which rotates inside the Gimbal, is the very core of the raster-scan structure. It supports the collimator and the X-ray source by means of two sets of opposing trusses before and after the declination pivot. The trusses are designed to have an equal amount of flexure, which allows the optics to stay on a common optical axis with the X-ray source. It also hosts tip / tilt metrology.
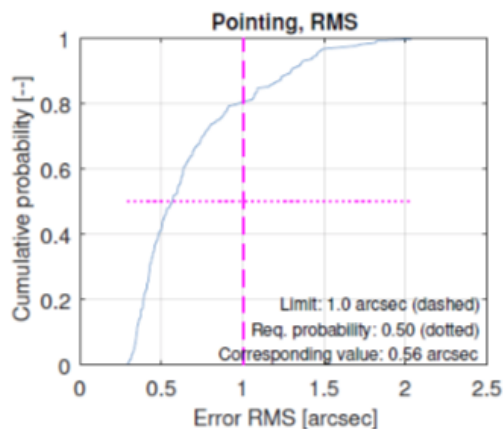


Figure 3. Cumulative probability of the RMS error in the various test sessions.

The raster-scan pointing error budget calculation has been performed through detailed simulation of calibration measures. Simulations are based on a proprietary tool by EIE called ErrorCalc, used for the design of astronomical telescopes, which has been updated and adapted for the purposes of VERT-X. Output of the simulations are reported in Fig.3 in terms of the cumulative probability of the RMS pointing error in the various test sessions. The median of the curve (0.56") is the final error estimation to be compared with the specification limit of 1". The figure shows that the error RMS is below the specification limit, thus the proposed raster-scan design is acceptable, with a scan velocity in the of 10-30 mm/s range.

In case of continuous scanning, considering a MA diameter of 2400 mm, a scanning speed of 20 mm/s, and a scanning step of 30 mm (which is the preliminary value of the X-ray beam width), the total scanning length is 1.2 km, and the total scanning time is ~2 hours. This value does not take into account the time for starting and stopping at every scanning row. This can be assessed only through a servo analysis, to understand what is the time and travelling space to damp down the transitory oscillations. It is expected to be of the order of 10s (per step), meaning 0.25 hr in total.
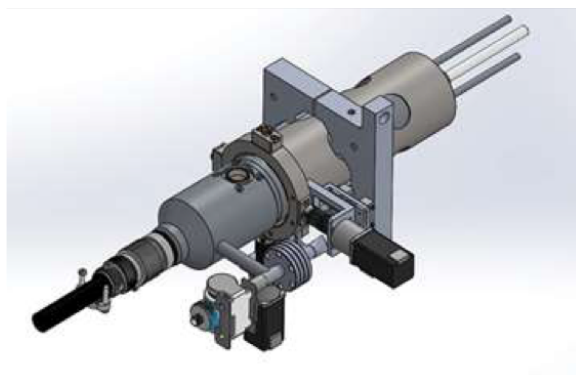
## 3.2 The X-ray source



Figure 4. The SIGRAY FAAST micro-focus X-ray source.

The X-ray source should provide a Bremsstrahlung spectrum in the 0.1 -12 keV energy range, with the most compelling requirement on its size. In fact, in order to keep the beam divergence in the order of 1", at a distance from the collimator of $\sim$ 2m, the size of the source should be of the order of 10$\mu$m. Among the sources on the market, the SIGRAY FAAST micro-focus X-ray source (Fig.4) turned out to be compliant with our needs. Indeed it can be mounted on the raster-scan mechanism and moved within the vacuum chamber. Its main characteristics are reported in Fig.4.

Table 1. SIGRAY FAAST X-ray source basic characteristics.

| PARAMETER | VALUE |
|---|---|
| Power | 0-100 W |
| Voltage | 20-50 kV |
| Size | 15$\mu$m (FWHM) at 50W |
| Targets | 5 different targets can be selected |
| Flux | $\sim 2 \times 10^{10}$ ph mm$^{-2}$ mrad$^{-1}$ |
| Window | Be |

## 3.3 The collimator

The proposed optical design of the X-ray collimator is based on a Wolter I configuration of about 1.1 m in length and an average grazing incidence angle of about 0.4°. This design is the result of a tradeoff analysis among different configurations that are briefly described below.
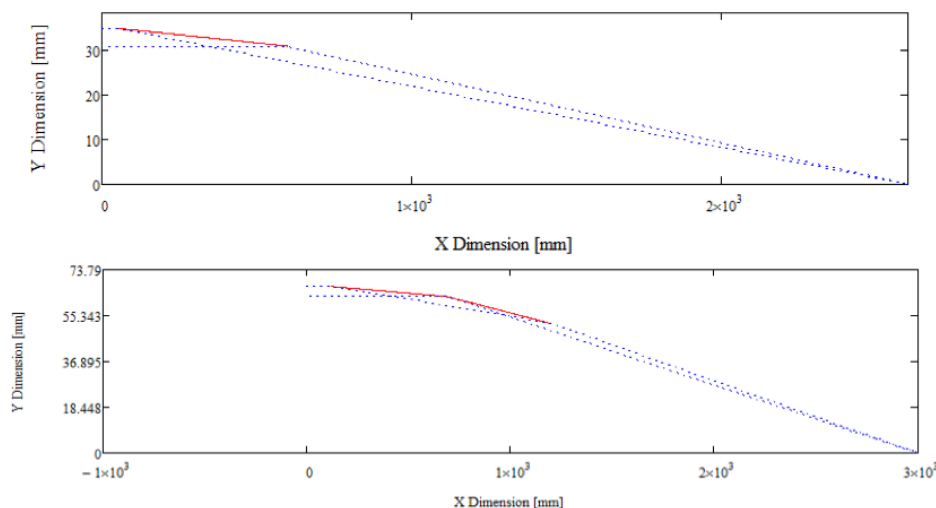


Figure 5. Optical layout of the two designs considered in the trade-off study: parabola single reflection in the upper panel and Wolter double reflection lower.

The main driving requirements that led to the definition of the optical design of the collimator are related to the needs of sufficiently high reflectivity in the spectral range between 0.2-12 keV and the limitation to 1" for the divergence error of the collimated beam produced by the mirror. The reflectivity requirement limits the average grazing incidence angle to less than 0.4°. Moreover, since micro-focus X-ray sources have dimension limited to 10-15 $\mu$m FWHM, the divergence requirements in turn limits the minimum distance between the source and the optics to about 2m.

Table 2. Summary of the mirror optical parameters.

| PARAMETER | VALUE |
|---|---|
| Min. distance of mirror from source (on axis) | 1800 mm |
| Min. collected angle | 1.56 ° |
| Max. collected angle. | 1.86° |
| Mirror length. | 1083 mm |
| Min. radial distance of the beam from axis. | 52.14 mm |
| Radial extension of the beam | 4.06 mm |

Given the above constraints, a possible collimator may consist of a section of a parabolic mirror collecting X-rays emitted in a small angular range around 0.8° at about 2 m from the source. The optical layout of the mirror is shown in the upper panel of Fig.5. This is similar to the case of BEATRIX [3].An alternative design, based on a Wolter I configuration, has been derived assuming the same collected angular range from the source. Since the grazing incidence angle of a Wolter mirror is roughly half that of a parabolic collimator, at equal collected angle from source, we doubled the latter, maintaining the average grazing incidence angle at about 0.4 °. The resulting design is shown in the lower panel of Fig.5. As expected, the length of the mirror is of the order of 1 m. Relevant design parameters and performance are listed in Tab 2.
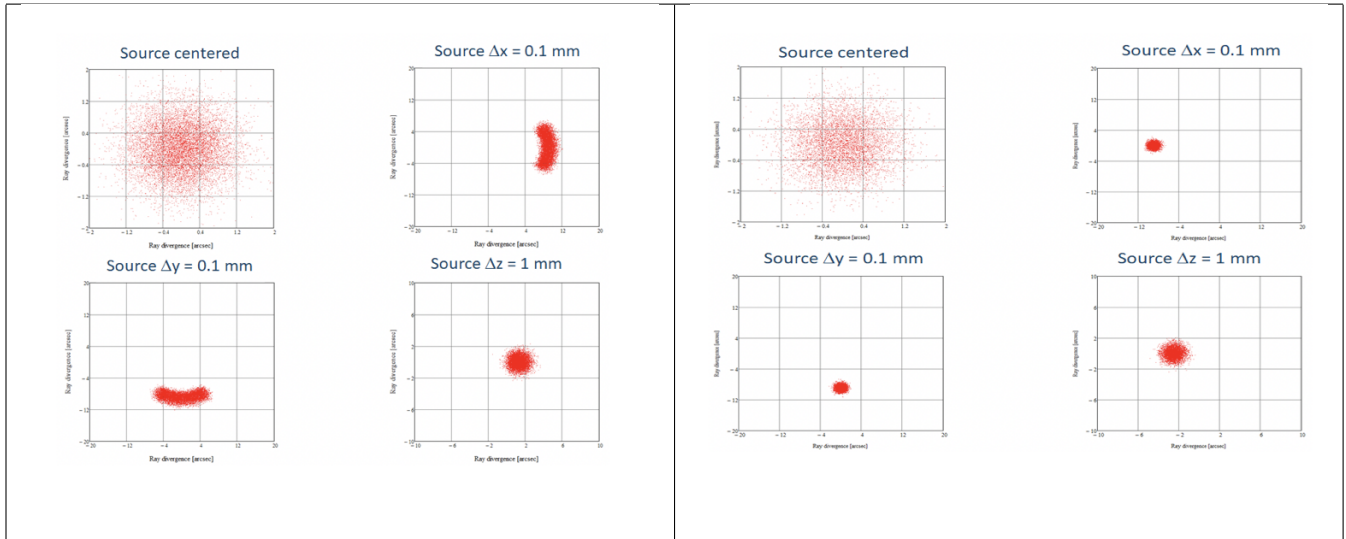


Figure 6. The results of the ray tracing simulation to assess the beam collimation sensitivity to alignment and source dimension, for parabola (left panel) and Wolter (right panel) designs. The off-axis divergence of each ray after collimation by the mirror is plotted in arcseconds.

The two designs have been further investigated in terms of sensitivity to source-to-mirror alignment and to source dimension. The collimation of the output beam from the collimator has been simulated by ray tracing assuming a 2D Gaussian distribution of the source with $15\mu$m FWHM both perfectly centered at collimator focus and displaced by 0.1 mm in X and Y (directions normal to optical axis) and 1 mm in Z (optical axis).

The results of the ray tracing simulation are shown in Fig.6. The off-axis divergence of each ray after collimation by the mirror is plotted in arcseconds (as such, a perfectly collimated beam would be represented by just one single point). In all plots the output beam is assumed to be 20 mm wide in the azimuthal direction. It can be concluded that the parabolic collimator is especially sensitive to the source dimension when combined to alignment errors transversal to the optical axis. It can also be noted that the position of the centroid of the beam is approximatively the same for the parabolic and Wolter collimator when the source is shifted in X and Y; however, the spread of the beam is much worse for the parabolic mirror.
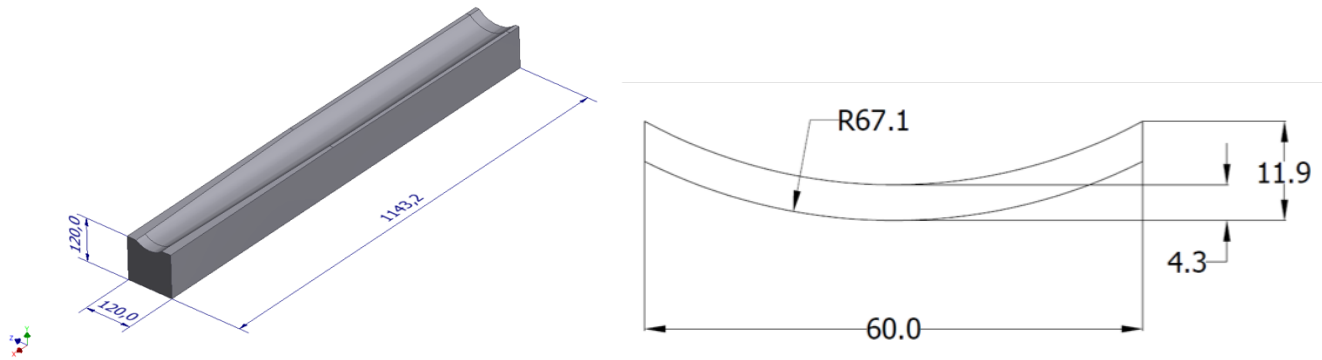
Figure 7. Preliminary mechanical design of the collimator, with dimensions expressed in mm.

A preliminary mechanical model has been defined and structural analysis has been performed to validate the concept of the VERT-X Wolter collimator. Zerodur® or equivalent is assumed as the collimator material. Overall mass is approximately 36.9 kg. General dimensions are reported in Tab.2. The total optical length of the optical area of the mirror is 1103.2 mm; it provides a collimated x-ray beam with a size shown in the next picture, whose illumination area is about 4.3 mm x 60 mm, corresponding to 258 mm² (Fig.7).

## 3.4 Mirror assembly supports and gravity mitigation

From the structural point of view the ATHENA MA is a monolithic structure made in titanium alloy, consisting in a sort of spatial frame, composed of thin walls surrounding fully open cells, which constitute the MMs housings. Given the very tight requirements the MA structure stiffness could be not intrinsically sufficient to fully contrast gravity distortions, when simply supported in kinematic mount conditions or when supported just at the outer edge. Furthermore functional requirements resulting from the optical design pose additional constraints to MA structure design. For instance, the MM pattern does not permit to have continuous radial walls (except in six azimuthal locations 60 deg. spaced). Discontinuous radial walls result in reduced stiffness performances. It follows that a dedicated and optimized supporting system (the gravity mitigation support system), to mitigate the gravity distortions will be needed. The gravity mitigation consists in a supporting system contrasting
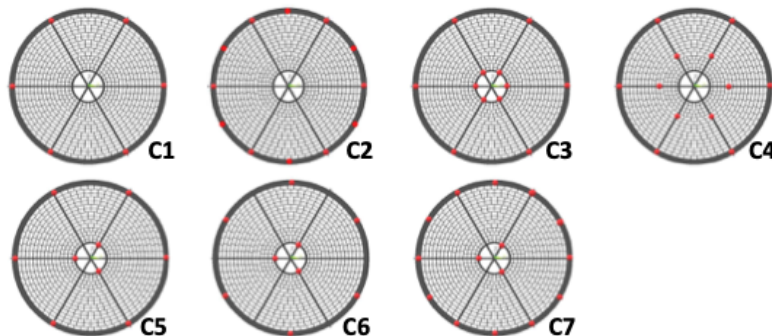


Figure 8. Different options of support pattern are shown.

axial gravity effects, limiting the PSF degradation induced by gravity during alignment/integration, testing and calibration. In VERT-X design the MA support system will be the same used during the mirror integration phase. This is possible because both these activities (calibration and integration) are carried out under axial gravity (gravity parallel to optical axis). In this way any additional distortion related to changes in the support pattern and/or in gravity direction is avoided.

Due to strategies adopted during integration and testing the main gravity impact on PSF is the gravity release after launch. The MA distortions related to gravity release, for different possible gravity mitigation support systems, are investigated by FEA. MM misalignments related to MA distortions are then post-processed by ray-tracing, to assess the impact on PSF. Both perfect MMs or MMs having 4.3" intrinsic errors will be used in ray-tracing.

Table 3. Expected impact of the gravity release on the HEW of a theoretical error- free mirror (second column) and on a realistic MM, with HEW of 4.3" (third column).

| Conf. | HEW (no error) | HEW ($HEW_{MM}$=4.3") |
|---|---|---|
| C1 | 0.527" | 4.353" |
| C2 | 0.484" | 4.327" |
| C3 | 0.096" | 4.303" |
| C4 | 0.056" | 4.302" |
| C5 | 0.109" | 4.305" |
| C6 | 0.110" | 4.308" |
| C7 | 0.109" | 4.306" |

To fullfill requirements the HEW related to gravity release has to be far lesser than 1". In Tab.3 seven different axial support patterns, two without and five with internal supports, are compared. They are also shown in Fig. 8.

Configurations C1 and C2, having respectively 6 or 12 supports evenly distributed along the outer ring, (with no internal supports) entail about 0.5 arcsec HEW at gravity release. With internal supports, several configurations are possible, with similar results in terms of PSF degradation at gravity release. For such patterns gravity release HEW at nominal focus ranges from 0.056 to 0.110". The minimum PSF degradation is given by the pattern C4 (Fig.8 ). Such pattern requires six axial supports along the outer ring and six inner supports at the intersection between ring 6 and the spokes. However, performance become homogeneous when intrinsic MM error (4.30" HEW) is summed to gravity release effects.

## 3.5 Metrology
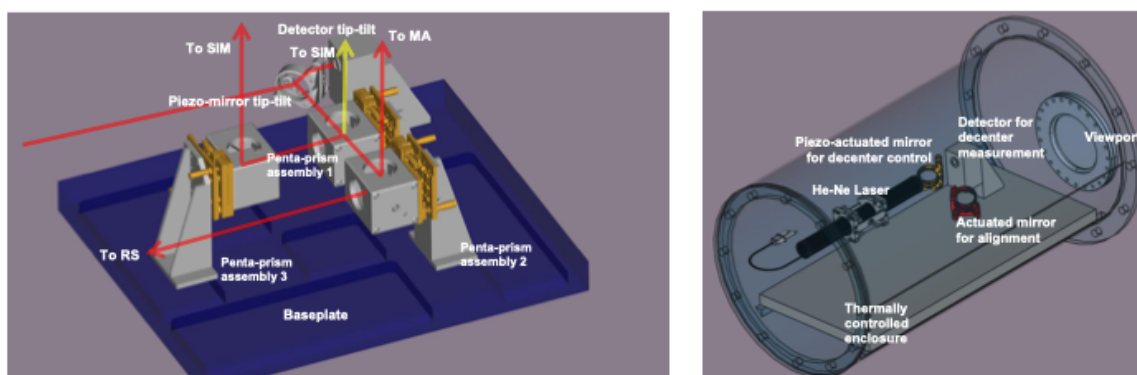


Figure 9. **Left panel:** Internal part of the ILDM. **Right panel:** External part of the ILDM.

The purpose of the VERT-X metrology system consists in keeping the alignment of the three main elements interested by the measurement: collimator, MA and Detector. Two different metrologic systems are included in the design: the linear displacement metrology (ILDM) and the tip-tilt metrology (TTM).

The ILDM system measures the linear displacement of a laser beam projected towards the MA and the SIM. Among this type of metrology, the best configuration is achieved with the laser beam placed outside the vessel.

In this way it is possible to take advantage of the large distance between the laser emitter and the piezo-actuated mirror / quad-cell detector combination, to accurately control the laser beam pointing direction.

The ILDM concept includes two parts. An external part, attached to the vessel, which contains the laser emitter and the system for decenter correction (right panel of 9). An internal part, anchored to the bottom of the XRS, which includes the system for tip-tilt stabilization and all the opto-mechanics needed to split the beam so to reach the MA and the SIM locations (left panel of 9).

As shown in Fig.10, in the overall layout of the TTM several subsystems are included. Three couples of two axis vacuum compatible tilt-meter (model 755 High Gain, vacuum compatible version, by Jewell Instruments) attached on MA, detector and raster-scan respectively. The raster-scan is also equipped with an optical tip-tilt detection system, which is includes two separated optical paths, one for each rotational degree of freedom. Both roll and pitch detections are based on an external roll detection station, the roll vacuum optical train and the roll reference mirror, which are mutually referenced in such a way to measure the rotations with respect to a unique reference.
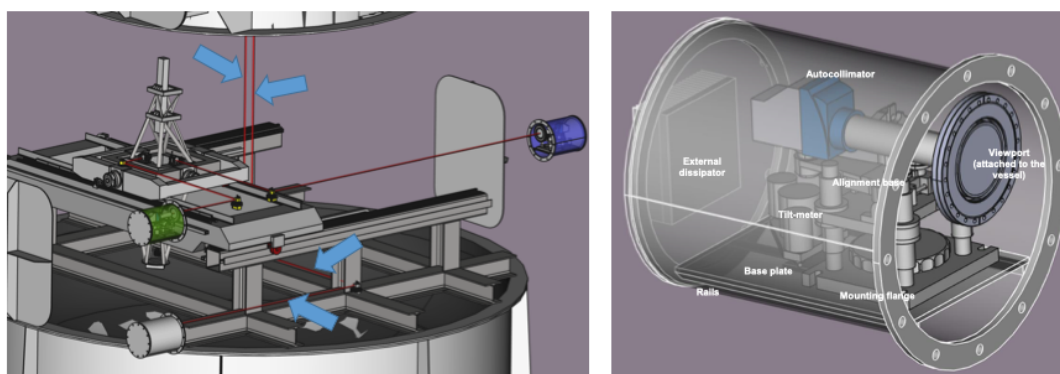


Figure 10. **Left panel:** Internal part of the TTM. **Right panel:** External part of the TTM.

## 3.6 The detector

The detector is a key element for any calibration facility. In particular, the time necessary to accomplish the calibration and verification tasks directly depends on the sustainable count rate and on its dimension. Moreover, the pixel size must adequately sample the ATHENA PSF and it should be fully compatible with vacuum operations.

Table 4. Sydor FastCCD detector basic characteristics.

| PARAMETER | VALUE |
|---|---|
| Energy range | 0.2 - 20 keV |
| QE 2keV | 70%. |
| QE 12keV | 40% |
| Pixel size | 30 $\mu$m (0.5" at 12m) |
| Sensor format | 960x960 pixels |
| Sensitive area size | 28.8 $\times$ 28.8 mm$^2$ |
| Max frame rate | 120 frame/s |
| Read-out noise rms | 24 e- |
| Vacuum compattibility | $<10^{-7}$Torr |

Given also the required range of sensitivity and a moderate energy resolution, commercial solutions based on soft x-ray silicon sensor with photon counting capabilities have been investigated. In particular, a critical trade-off

needs to be evaluated between the readout noise (affecting the energy resolution and the low energy threshold in photon counting mode) and the frame rate (which is strictly related to the maximum sustainable flux). Given that, as the best option on the market we selected the Sydor FastCCD detector.
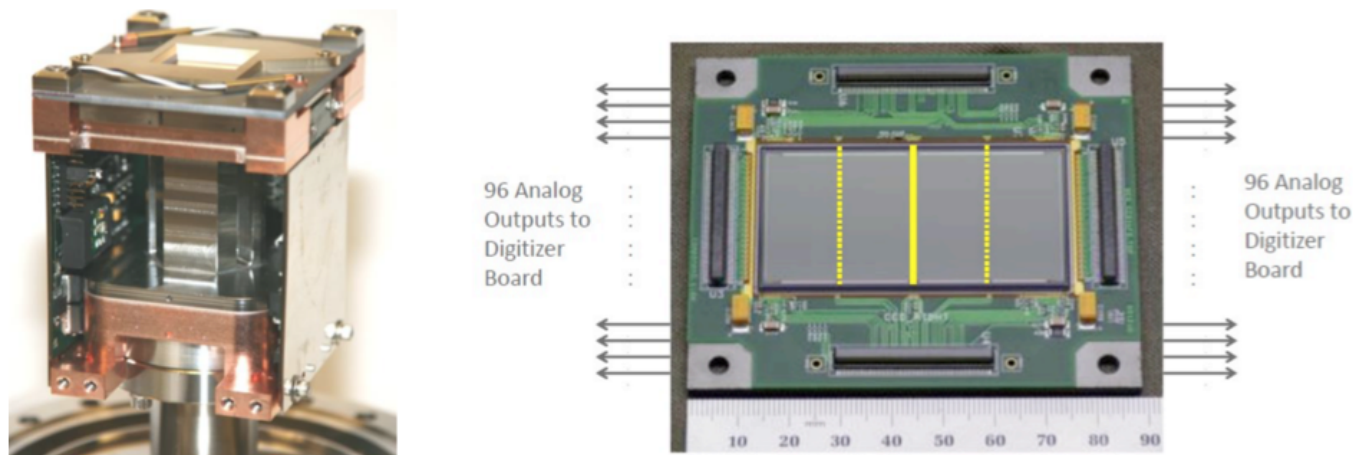


Figure 11. Overview of the CCD and the camera head.

The Sydor camera main blocks are (i) the vacuum-compatible camera head, (ii)the cooling subsystem, (iii) the power supply subsystem and (iv) the data acquisition readout system. The camera head includes the sensor, the front-end electronics and the the mechanical mounting with a temperature stabilization subassembly.

The sensor is a custom, LBNL developed, back-side illuminated, fully depleted CCD manufactured using the Teledyne/Dalsa 150mm C25 2.5 $\mu$m process. The sensor area is a 960 x 1920 array of $30\mu$m pixels and can be used as a 960 x 960 pixels split frame store device, i.e. with the sensitive area at the centre of the device and two storage sections at the top and at the bottom (Fig.11 ). To provide maximum sensitivity for soft X-Rays, the sensor is thinned to $200\mu$m and then ion-implanted on the back side with a 10 nm entrance window to provide transmission efficiencies of greater than 75% from 200eV, 95% at 600eV, and approaching 99% at 1keV. The readout architecture is highly parallel, with 96 outputs on each of both sides (one every 10 columns, with each column splitted on two outputs). The front-end electronics is based on custom ASICs developed at LBNL (fCRIC), allowing a very high frame rate with moderate readout noise ($< 25$ e- at 120 frames/s full frame). The time required to move the charges from the active area to the storage area with the current sensor is tt=500 $\mu$s. Photons arriving during this time will be misallocated in the direction of the transfer: to avoid photons impinging the sensor during this time it is possible to use a shutter: in this case tt is the minimum dead time. The noise of the FastCCD camera in the current commercial model has been reduced with fibre-optic cabling but it is still moderately high (24 e-). The noise affects two parameters, the photon counting detection threshold and energy resolution. In particular at this level calibration test under 0.7 keV cannot be performed in photon counting mode. Alternative solutions are under scrutiny. One possibility is performing the low-energy tests in imaging mode, which would require a highly monochromatic input source. The best option will be probably reducing the frame rate in order to test low energy with lower noise.

Assuming the pixel size of 0.5" at the ATHENA focal length of 12m and HEW of 5", we can estimate the photon rate per frame producing significant pile-up. This has been done bootstrapping the ATHENA PSF and estimating the probability of having two events in the same 3x3 pixel window. In Fig 12 we show that pileup level is under the requirement of 1% up to 0.4 photons per frame: this means that with FastCCD camera operated at 100 frames s$^{-1}$ we can safely handle photon count rate up to 40 count s$^{-1}$.

The detector will be moved for several reasons during the calibration operations. First along the direction parallel to the optical axis in order to perform out of focus measure as foreseen by the calibration plan. Then, since the
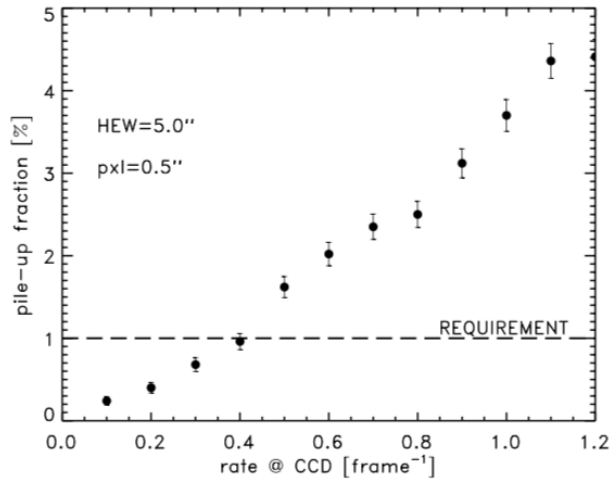
Figure 12.  The pile-up level as function of the rate of photons per frame. The 1% requirement is also shown.

detector is smaller than the field of view, translation within the focal plan will be necessary to test both the off-axis performance and the stray-light contamination.

Finally, a translation of the order of $\sim 60$ cm will be included for the purposes of the effective area calibration. In fact, calibration of the MA effective area can be achieved as the ratio of the focused beam with the beam directly incident on the detector. For the direct beam, the easiest path would be, of course, through the central aperture in the MA. However, if this will not be possible, an alternative solution would be exploiting the aperture of one single mirror module before the integration. In this case the detector stage will have to guarantee an additional translation in the focal plane.
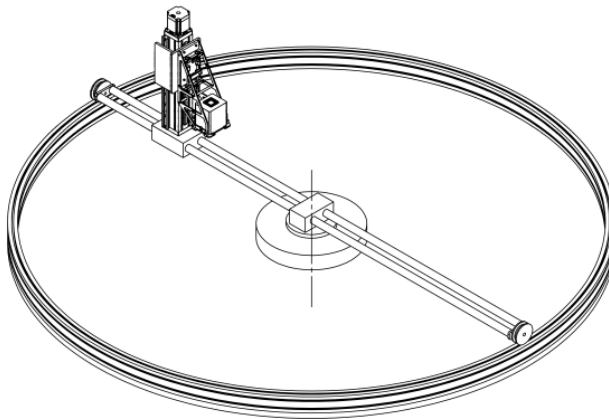


Figure 13.  The detector stage preliminary design.

## 4. THE HEW ERROR BUDGET

A point-like source located in the focus of an error free X-ray collimator, would theoretically produce a perfectly parallel beam which would allow to directly measure the ATHENA HEW ($\mathrm{HEW_{MA}}$). In practice, the HEW measured at VERT-X ($\mathrm{HEW_{VTX}}$) will be the quadratic sum of $\mathrm{HEW_{MA}}$ plus several independent contributions:

the source dimension $\mathrm{HEW_{SOU}}$, the mirror error $\mathrm{HEW_{MIR}}$, the pointing uncertainty $\mathrm{HEW_{PNT}}$ and the gravity induced distorsion, $\mathrm{HEW_{GRV}}$.

$$\mathrm{HEW^2_{VTX}} = \mathrm{HEW^2_{MA}} + \mathrm{HEW^2_{SOU}} + \mathrm{HEW^2_{MIR}} + \mathrm{HEW^2_{GRV}} + \mathrm{HEW^2_{PNT}}\,, \tag{1}$$

The uncertainty on the $\mathrm{HEW_{MA}}$ will be given by the sum of the uncertainties of each single term, weighted by the ratio with the intrinsic $\mathrm{HEW_{MA}}$.

$$\sigma^2_{\mathrm{MA}} = \frac{\mathrm{HEW^2_{VTX}}}{\mathrm{HEW^2_{MA}}}\sigma^2_{\mathrm{VTX}} + \frac{\mathrm{HEW^2_{SOU}}}{\mathrm{HEW^2_{MA}}}\sigma^2_{\mathrm{SOU}} + \frac{\mathrm{HEW^2_{PNT}}}{\mathrm{HEW^2_{MA}}}\sigma^2_{\mathrm{PNT}} + \frac{\mathrm{HEW^2_{MIR}}}{\mathrm{HEW^2_{MA}}}\sigma^2_{\mathrm{MIR}} + \frac{\mathrm{HEW^2_{GRV}}}{\mathrm{HEW^2_{MA}}}\sigma^2_{\mathrm{GRV}} \tag{2}$$

This error has to be compared with the calibration goals which require an HEW error of 0.1" [8]. Values of single terms have been previously discussed in the corresponding sections of the paper and are summarised here in Tab 5. It is evident that the main contribution to the final uncertainty is the measure error of $\mathrm{HEW_{VTX}}$,

Table 5. HEW error budget.

| ELEMENT | VALUE |
|---|---|
| $\mathrm{HEW_{MA}}$ | 5.0" |
| $\mathrm{HEW_{SOU}}$ | 1.0" |
| $\mathrm{HEW_{MIR}}$ | 0.5" |
| $\mathrm{HEW_{PNT}}$ | 0.6" |
| $\mathrm{HEW_{GRV}}$ | 0.2" |

which is the statistical error, being the only one with a weight $\sim 1$. Since the other terms are of the order of $\lesssim$ 1", they contribute with significantly smaller weights to the error budget. Even with uncertainties at 20-30%, they do not significantly contribute to the final uncertainty $\sigma_{\mathrm{MA}}$ (Eq.2).
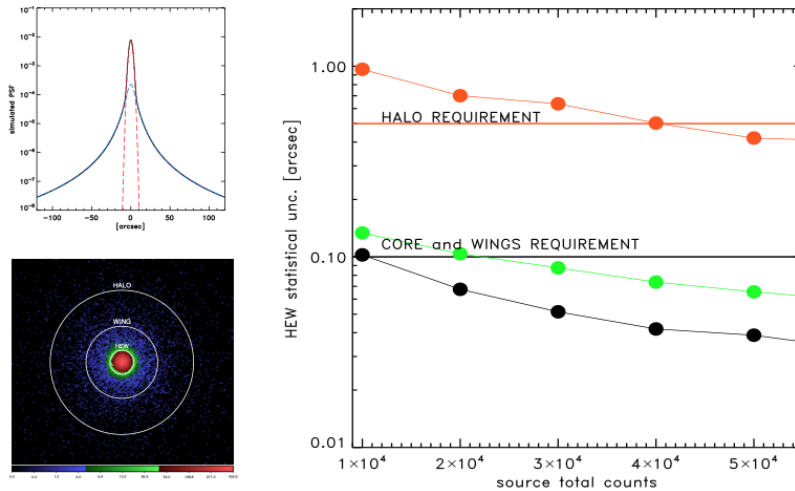


Figure 14. Left panels: the PSF assumed in order to calculate the expected calibration statistical errors. Right panel: the measure statistical uncertainties as function of the number of photons, with the calibration requirements for HEW, wings and halo respectively .

The statistical error directly depends on the number of photons accumulated in the calibration measure. Calibration accuracy on the PSF is required for the HEW (0.1", as already mentioned), for the wings (3 times the

HEW) and for the halo (6 times the HEW). Assuming a PSF with a central gaussian profile with HEW=5",
wings and halo similar to the XMM PSF, we estimate that requirements on HEW and PSF wings can be met
by 10,000 photons. It results that the most tight requirement is the one on the PSF halo, with a minimum of
40,000 photons to fulfill the 0.5" reqirement (Fig.14).

## 5. SUMMARY AND CONCLUSIONS

We presented the concept design of VERT-X, with particular focus on the most original aspects of the project,
namely the X-ray source - collimator subsystem and the raster-scan mechanism. According the current design,
the VERT-X facility fulfils the ATHENA requirements both in terms of PSF and effective area calibration with
the expected systematic error sources being at the level of $\lesssim$ 1". If equipped with the appropriate detector
(with a sustainable count rate of 10-40 ph s$^{-1}$) the ATHENA MA calibration tasks with the required statistical
uncertainty can be completely accomplished in the required time (6 months, contingencies included). In addition
to the lower costs, the compactness of the VERT-X design produces some benefits with respect to a long tube
facility. First, the vertical geometry largely simplifies the mirror support. Moreover, several different options for
the location of the facility can be considered. In particular the possibility of building VERT-X in proximity of
the MA integration facility seems very attractive from different points of view especially security, time and cost.
This option is currently under study and will be presented in the next future.

## 6. REFERENCES

[1] Nandra, K., Barret, D., Barcons, X. et al., "The Hot and Energetic Universe: A White Paper presenting the
science theme motivating the Athena mission", arXiv:1306.2307.

[2] Bavdaz, M., Wille, E., Ayre, M., Ferreira, I. et al., "Development of the ATHENA mirror," in [Space
Telescopes and Instrumentation 2018: Ultraviolet to Gamma Ray], Society of Photo-Optical Instrumentation
Engineers (SPIE) Conference Series 10699, 106990X (Jul 2018).

[3] Salmaso, B., Spiga, D., Basso, S. et al., "Progress in the realization of the beam expander testing x-ray facility
(BEaTriX) for testing ATHENA's SPO modules," in [Space Telescopes and Instrumentation 2018: Ultraviolet
to Gamma Ray], Society of Photo-Optical Instrumentation Engineers (SPIE) Conference Series 10699, 106993I
(Jul 2018).

[4] Valsecchi, G., Marioni, F., Bianucci, G. et al., "Results of silicon pore optics mirror modules optical integration
in the ATHENA telescope," in [Space Telescopes and Instrumentation 2018: Ultraviolet to Gamma Ray], Society
of Photo-Optical Instrumentation Engineers (SPIE) Conference Series 10699, 106990Z (Jul 2018).

[5] Guainazzi, M. and et al., "ATHENA Mirror Calibration Plan " – ESA-ATHENA-ESTEC-SCI-PL-0001

[6] Burwitz, V., Willingale, R., Pellilciari, C. et al., "Testing and calibrating the ATHENA optics at PANTER
(Conference Presentation)," in [Society of Photo-Optical Instrumentation Engineers (SPIE) Conference Series],
Society of Photo-Optical Instrumentation Engineers (SPIE) Conference Series 10399, 103990O (Sep 2017).

[7] Pareschi, G., Moretti, A., Salmaso B. et al., "A vertical facility based on raster-scan configuration for the
x-ray scientific calibrations of the athena optics", Proceedings Volume 11180, International Conference on Space
Optics - ICSO 2018.

[8] Guainazzi, M., "Athena optics calibration plan", IACHEC meeting 2019.